Cancer Cell
Article

VCAM-1 Promotes Osteolytic Expansion of Indolent Bone Micrometastasis of Breast Cancer by Engaging α4β1-Positive Osteoclast Progenitors

Xin Lu,[1] Euphemia Mu,[1] Yong Wei,[1] Sabine Riethdorf,[2] Qifeng Yang,[3,4] Min Yuan,[1] Jun Yan,[1] Yuling Hua,[1] Benjamin J. Tiede,[1] Xuemin Lu,[1] Bruce G. Haffty,[3,5] Klaus Pantel,[2] Joan Massagué,[6,7] and Yibin Kang[1,4,*]
[1]Department of Molecular Biology, Princeton University, Princeton, NJ 08544, USA
[2]Department of Tumor Biology, University Medical Center Hamburg-Eppendorf, D-20246 Hamburg, Germany
[3]Department of Radiation Oncology, Robert Wood Johnson Medical School, University of Medicine and Dentistry of New Jersey, New Brunswick, NJ 08901, USA
[4]Department of Breast Surgery, Qilu Hospital of Shandong University, Jinan, Shandong Province 250012
[5]Cancer Institute of New Jersey, New Brunswick, NJ 08903, USA
[6]Cancer Biology and Genetics Program
[7]Howard Hughes Medical Institute
Memorial Sloan-Kettering Cancer Center, New York, NY 10021, USA
*Correspondence: ykang@princeton.edu
DOI 10.1016/j.ccr.2011.11.002

SUMMARY

Breast cancer patients often develop locoregional or distant recurrence years after mastectomy. Understanding the mechanism of metastatic recurrence after dormancy is crucial for improving the cure rate for breast cancer. Here, we characterize a bone metastasis dormancy model to show that aberrant expression of vascular cell adhesion molecule 1 (VCAM-1), in part dependent on the activity of the NF-κB pathway, promotes the transition from indolent micrometastasis to overt metastasis. By interacting with the cognate receptor integrin α4β1, VCAM-1 recruits monocytic osteoclast progenitors and elevates local osteoclast activity. Antibodies against VCAM-1 and integrin α4 effectively inhibit bone metastasis progression and preserve bone structure. These findings establish VCAM-1 as a promising target for the prevention and inhibition of metastatic recurrence in bone.

INTRODUCTION

One mysterious feature of metastases is that distant relapse can occur many years after successful primary tumor removal and clinically disease-free survival (Aguirre-Ghiso, 2007). The latency before distant metastasis relapse is defined as metastasis dormancy. Understanding the mechanism of dormancy and its reactivation has important clinical implications for controlling metastatic progression and maintaining patients in a disease-free state (Chambers et al., 2002; Goss and Chambers, 2010). In preclinical models, cancer can remain dormant either as quiescent cells (cellular dormancy) or as indolent small clusters that maintain balanced proliferation and death (tumor mass dormancy) (Aguirre-Ghiso, 2007). Various possible mechanisms of dormancy have been suggested based on studies performed in preclinical models, including inefficient angiogenesis, antibody- or T cell-mediated immune surveillance, lack of proliferative signals, and the activity of metastasis suppressor genes and microRNAs, although the extent to which these mechanisms reflect clinical dormancy is unclear (Aguirre-Ghiso, 2007; Goss and Chambers, 2010). Clinical dormancy in patients has been extensively studied in breast cancer. Time distribution analyses of both mortality and recurrence showed an early polynomial-like curve and a late persistent rate for up to more than 20 years

Significance

The transition from dormant micrometastasis to overt macrometastasis represents a crucial turning point in breast cancer. Significant advances have been made to characterize the complex tumor-microenvironment interactions in overt bone metastasis. However, the molecular and cellular events that drive the early events of bone metastasis—the activation of indolent micrometastasis—remain poorly understood. Our study reveals a mechanism for tumor cells to escape dormancy whereby monocytic osteoclast progenitors are recruited through vascular cell adhesion molecule 1 (VCAM-1)-α4β1 binding to produce a localized increase of osteoclast activity and initiate the cycle of bone destruction and tumor growth. VCAM-1- or α4-blocking antibodies effectively inhibit bone metastasis, suggesting that VCAM-1 is a promising therapeutic target to restrict the progression of micrometastasis in bone.

(Demicheli et al., 1996). Interrupted and prolonged dormancy was proposed to explain the bimodal pattern (Demicheli, 2001), yet with little molecular insight.

Postoperative distant recurrence arises invariably from disseminated tumor cells, which are often found in the bone marrow of breast cancer patients without any clinical sign of metastasis (Braun et al., 2005; Klein, 2009). Bone metastasis is a frequent complication of breast cancer and is often accompanied by debilitating bone fracture, severe pain, nerve compression, and hypercalcemia (Weilbaecher et al., 2011). Bone metastasis is characterized by the intricate interaction between tumor cells and bone microenvironment. In breast cancer, continuous expansion of osteolytic bone metastasis is driven by the "vicious cycle" of tumor-dependent activation of bone-degrading osteoclasts and bone stroma-dependent stimulation of tumor malignancy (Weilbaecher et al., 2011). Therefore, identification of tumor-derived osteoclastogenic factors may provide new potential therapeutic targets. Currently, it is unknown whether molecules involved in the vicious cycle are also important for driving the transition from indolent micrometastasis to overt metastasis in bone. This lack of understanding can be largely explained by the paucity of appropriate animal models that mimic the metastatic relapse process. Here, we report the establishment of a dormancy-reactivation model of breast cancer bone metastasis. Using this model, we linked osteoclast activation with the switch from micrometastasis to osteolytic macrometastasis, and identified vascular cell adhesion molecule-1 (VCAM-1) as a key regulator of this process.

VCAM-1 is a member of the transmembrane immunoglobulin superfamily (Osborn et al., 1989). Proteolytic shedding of VCAM-1 also generates a soluble form of VCAM-1 (Garton et al., 2003). The predominant receptor for VCAM-1 is integrin $\alpha4\beta1$ (i.e., very late antigen-4, VLA-4), which is expressed by many cell types of the hematopoietic lineage, including B and T lymphocytes, monocytes, eosinophils, and basophils (Carter and Wicks, 2001). VCAM-1 is expressed by cytokine-activated endothelial cells (Osborn et al., 1989) and VCAM-1-$\alpha4\beta1$ binding plays an important role in mediating leukocyte adhesion and transendothelial migration during inflammation (Springer, 1994), which may be the underlying mechanism for VCAM-1 function in rheumatoid arthritis (Carter and Wicks, 2001) and early atherosclerosis (Cybulsky et al., 2001). Aberrant expression of VCAM-1 in cancer cells was documented in preclinical models as well as patient samples of gastric cancer (Ding et al., 2003), renal cell carcinoma (Lin et al., 2007), and breast cancer (Chen et al., 2011). However, it is unknown whether tumor-derived VCAM-1 has any functional role in breast cancer metastasis to bone. Combining the power of functional genomics and a multiphoton imaging technique, ex vivo imaging of bone metastasis (EviBoM), we discovered a role of VCAM-1 in promoting the outgrowth of indolent bone micrometastasis and established VCAM-1 as a promising target for preventing metastatic recurrence in bone.

RESULTS

Identification of VCAM-1 as a Crucial Activator of Indolent Bone Micrometastasis

We previously used an in vivo selection strategy to derive bone-metastatic variants of the MDA-MB-231 breast cancer cell line in order to identify bone metastasis genes (Kang et al., 2003). Dilution cloning of the parental MDA-MB-231 population revealed a small percentage of pre-existing highly bone-metastatic cells that overexpress the bone-metastasis gene signature, including genes such as *CXCR4*, *IL11*, *CTGF*, *MMP1*, and *OPN* (Kang et al., 2003). Consistent with the functional importance of these genes, single cell-derived populations (SCPs) of MDA-MB-231 that lack the expression of the bone metastasis gene signature (e.g., SCP3, SCP4, SCP6, SCP21) were incapable of generating any X-ray-detectable bone metastases within 100 days after injection (Figures 1A and 1B; see also Figure 5B in Kang et al., 2003). However, after more than 4 months, a small percentage (~10%) of mice injected with SCP6 developed overt bone metastasis. Cell lines derived from such a bone lesion (e.g., postdormancy generation 1 [PD1]) possess drastically increased metastatic potential (Figures 1A–1C). Close monitoring of mice injected with luciferase-labeled SCP6 by the more sensitive bioluminescence imaging (BLI) revealed repeated failure of micrometastases in bone to expand to become overt macrometastases (Figure S1A available online, highlighted by yellow circles), in contrast to the rapid development of osteolytic lesions by highly bone-metastatic lines such as SCP25 (Figure S1A). This long "lead time" before the infrequent overt bone metastasis formation (Figure S1A, red circle) from indolent micrometastasis is similar to the clinical observation of metastatic dormancy and subsequent relapse. From the bone metastases formed by PD1, second-generation sublines (PD2) were isolated (Figure 1A). Most of the PD2 sublines (PD2A, PD2B, PD2C, PD2D, and PD2E) metastasize to bone as efficiently as PD1, whereas one subline, PD2R, significantly lost its metastatic potential and was therefore considered as a partial revertant to the dormant state (Figures 1B and 1C). These near-isogenic sublines that were derived from a common progenitor but had dramatic differences in metastatic abilities represented an ideal cohort to identify crucial drivers of outgrowth from indolent bone micrometastasis.

To ensure the lineage relationships between different sublines derived in this study and the parental MDA-MB-231, we analyzed genomic copy number changes using array comparative genomic hybridization (CGH) (Figure S1B). PD1 and SCP6 shared very similar chromosomal profiles to MDA-MB-231, suggesting that the dramatic differences in their metastatic abilities are not likely the result of gross genomic alterations or accidental contaminations from other cell lines.

Because the highly aggressive bone-metastatic ability of the PD sublines is similar to that of the MDA-MB-231 variants previously isolated from in vivo selection (Kang et al., 2003), we first tested whether the PD sublines activated the same bone metastasis signature (Kang et al., 2003). Surprisingly, none of the previously described bone metastasis genes was found to be upregulated in the PD sublines (Figures S1C and S1D), suggesting that an independent mechanism was developed by the PD cells to acquire the bone-metastatic ability. Microarray profiling revealed differentially expressed genes between the highly metastatic PD1/PD2 lines and the weakly metastatic lines (SCP3, SCP4, SCP6, MDA-MB-231, and PD2R) (Figures 1D and 1E; Table S1). Several genes overexpressed in PD1/PD2 lines have been implicated in breast cancer,

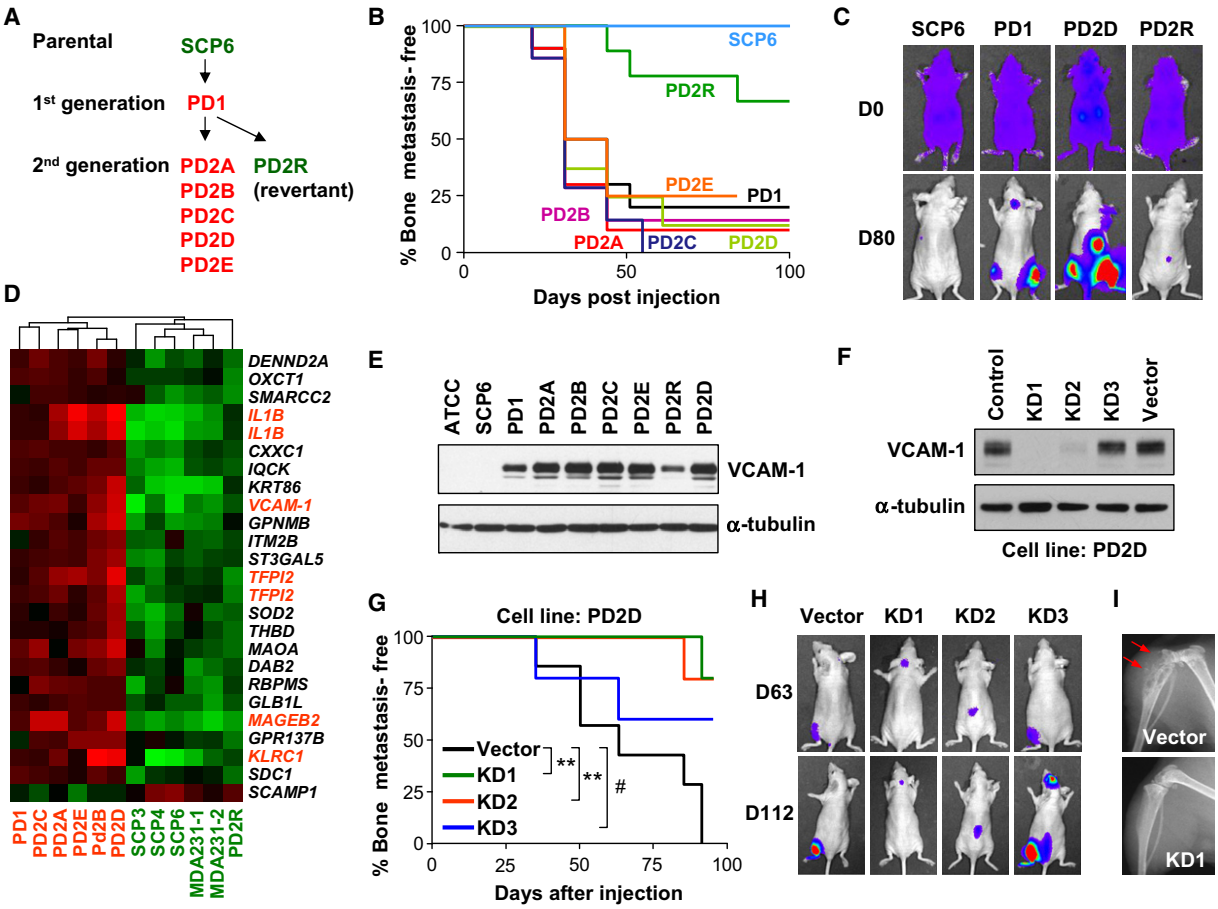

Figure 1. Identification of VCAM-1 as a Bone Metastasis Gene in a Mouse Model of Metastatic Dormancy and Activation

(A) Relationship of parental SCP6 and postdormancy (PD) sublines. Sublines with strong bone-metastatic ability are color-coded in red and sublines with weak bone-metastatic ability are color-coded in green.

(B and C) Kaplan-Meier curve of bone metastasis development of different cell lines with BLI of representative mice (n = 10).

(D) Supervised clustering of samples using genes differentially expressed between weak (green) and strong (red) bone-metastatic cell lines. Genes highlighted in red were functionally tested.

(E) Differential expression of VCAM-1 in parental and PD sublines as detected by western blot analysis.

(F) VCAM-1 KD in PD2D as detected by western blot analysis.

(G) Kaplan-Meier curve of bone metastasis development of the indicated PD2D cells (n = 8). $^{**}p < 0.01$, $^{\#}p > 0.1$ by log-rank test.

(H) Representative BLI of mice from (G) on day 63 and day 112.

(I) Representative X-rays with arrows pointing to osteolytic lesions. See also Figure S1 and Table S1.

including *IL1B* (Jin et al., 1997), *TFPI2* (Wojtukiewicz et al., 2003), *MAGEB2* (Lurquin et al., 1997), *KLRC1* (Minn et al., 2005), and *VCAM-1* (Minn et al., 2005). However, none of them has been previously linked to bone metastasis.

To determine whether one or more of these five genes contributed to metastasis, we used short hairpin RNAs (shRNAs) to stably silence each gene in a representative strongly metastatic PD line, PD2D. Knockdown (KD) of *IL1B*, *TFPI2*, *MAGEB2* or *KLRC1* had no effect on bone metastasis (Figure S1E). Three different *VCAM-1* shRNAs showed different KD efficiency (Figure 1F). Whereas KD1 and KD2 significantly reduced VCAM-1 expression, KD3 did not reduce VCAM-1 level (Figure 1F) and thus served as an additional negative control. The two efficient knockdowns significantly abolished the bone-metastatic ability (Figures 1G and 1H). X-rays (Figure 1I) revealed the osteolytic nature of the bone lesions formed by control cells and the attenuation of this phenotype in the KD cells. To further confirm the specificity of VCAM-1 KD, VCAM-1 expression was rescued in the KD1 subline by stably expressing an shRNA-resistant *VCAM-1* coding sequence (Figure 2A). When inoculated in vivo, the rescue cells showed recovered metastatic potential (Figures 2B and 2C). Collectively, these results suggest that VCAM-1 is essential for the acquired osteolytic bone-metastatic ability in the PD lines.

Acquisition of VCAM-1 Expression by In Vivo Evolution

Escape from metastasis dormancy was hypothesized to occur through adaptive changes of micrometastases (Weinberg, 2008), although this argument has not been supported by evidence collected from a mouse model with a natural history of metastatic progression from dormancy. Most previous metastasis models enriched subpopulations with inherently

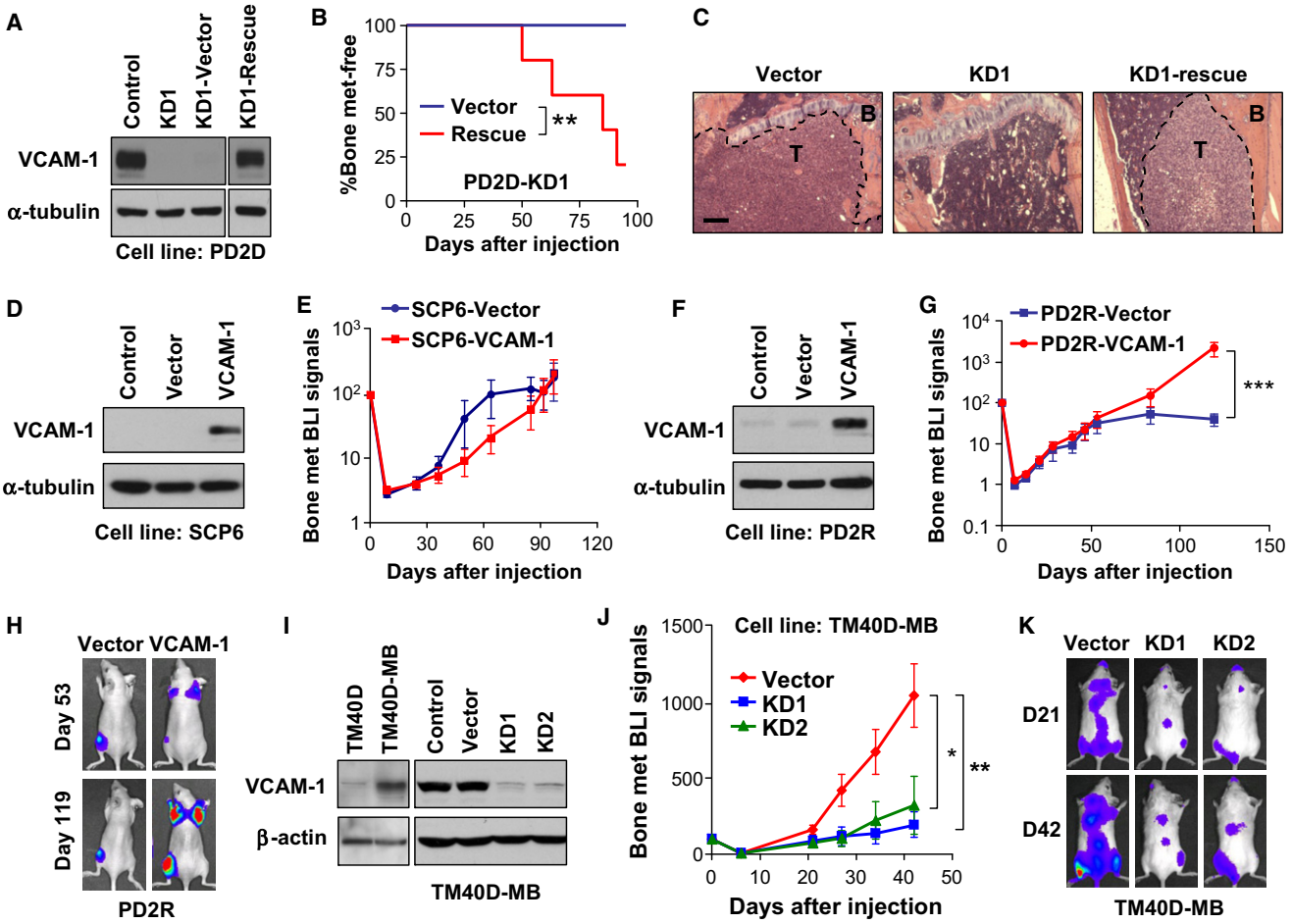

Figure 2. Essential Role of VCAM-1 in Bone Metastasis

(A) Rescued VCAM-1 expression in the VCAM-1-KD PD2D subline as detected by western blot analysis.

(B) Kaplan-Meier representation of bone metastasis relapse by control and VCAM-1-rescued cell lines in (A) (n = 6). **$p < 0.01$ (log-rank test).

(C) Hematoxylin and eosin staining of tibia showing presence or absence of overt metastatic tumors (T) in bone (B) by different tumor cells. Scale bar, 200 μm.

(D) Ectopic overexpression of VCAM-1 in SCP6 as detected by western blot analysis.

(E) BLI curves of in vivo bone metastasis assay with SCP6 variants. Data represent the mean ± SD (n = 6). No time point showed statistical significance (Mann-Whitney test).

(F) Ectopic overexpression of VCAM-1 in PD2R as detected by western blot analysis.

(G) BLI curves of bone metastasis development by control and VCAM-1-overexpressing PD2R cells. Data represent the mean ± SEM (n = 10). ***$p < 0.001$ (Mann-Whitney test).

(H) Representative BLI of mice in (G).

(I) Endogenous expression of VCAM-1 in the murine cell line TM40D and the subline TM40D-MB, and VCAM-1 KD in TM40-MB, as detected by western blot analysis.

(J) BLI curves of bone metastasis development by the indicated TM40D-MB cells. Data represent the mean ± SEM (n = 10). *$p < 0.05$, **$p < 0.01$ (Mann-Whitney test).

(K) Representative BLI of mice in (J) on day 21 and day 42. See also Figure S2.

stronger metastatic potential in a cell line through in vivo selection (Kang et al., 2003; Minn et al., 2005). Without the in vivo evolution of dormancy, this approach is unlikely to find genes critical for activation of overt bone metastasis from dormant micrometastases. To evaluate our model in this respect, we investigated whether VCAM-1 upregulation was a newly evolved event during the outgrowth from micrometastasis of SCP6. Highly abundant VCAM-1 protein was detected in aggressive PD lines with localization restricted to cell membrane (Figures S2A and S2B), allowing flow cytometric analysis of VCAM-1$^+$ cells. VCAM-1 expression pattern was examined exhaustively in SCP6 using fluorescence-activated cell sorting (FACS) analysis of 8.7 × 10^6 cells (Figure S2C). Only 17 cells were stained positive. This extremely low percentage of VCAM-1$^+$ cells was determined to be a false positive when the sorted VCAM-1$^+$ cells were expanded into a larger population and VCAM-1 expression was re-examined (Figure S2C). Therefore, we conclude that VCAM-1 upregulation most likely evolved in vivo during the natural metastasis progression from indolent micrometastasis to overt macrometastasis.

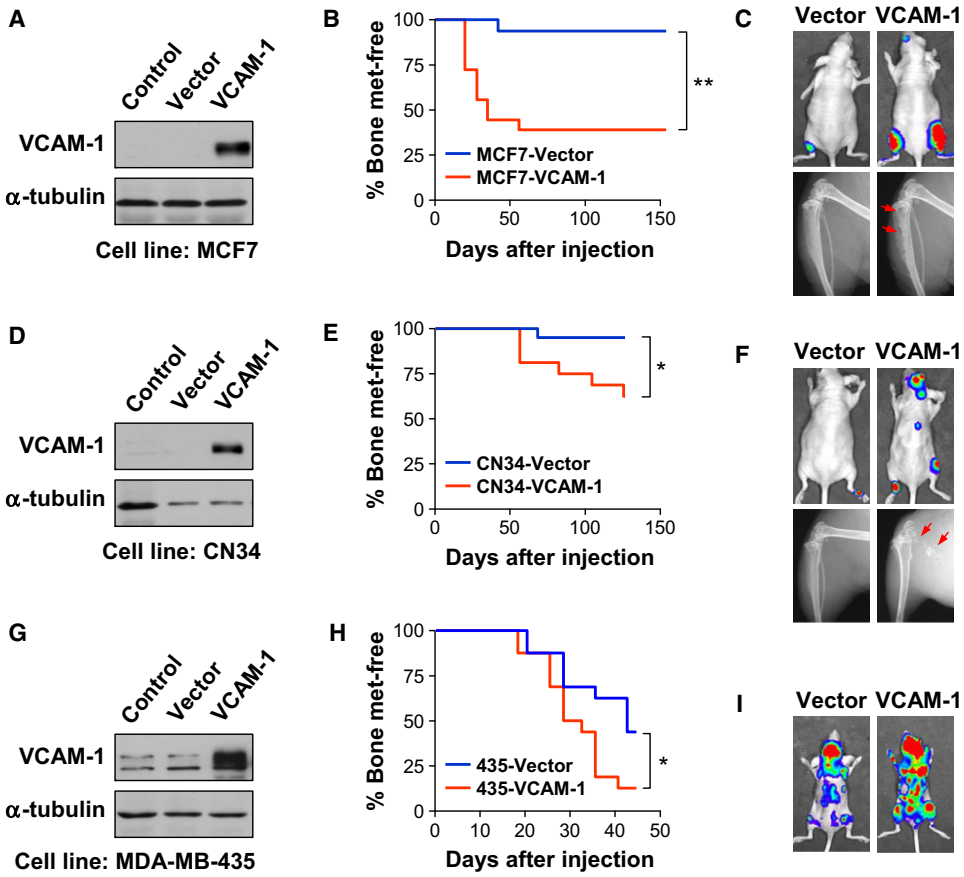

Figure 3. Prometastatic Activity of VCAM-1 in Additional Bone Metastasis Models

(A) Ectopic overexpression of VCAM-1 in MCF7 as detected by western blot analysis.

(B) Kaplan-Meier curve of bone metastasis development of control and overexpression MCF7 cells (n = 10). **p < 0.01 (log-rank test).

(C) Representative BLI (day 125) and X-rays (day 154) of mice from (B). Arrows point to osteolytic lesions.

(D) Ectopic overexpression of VCAM-1 in CN34 as detected by western blot analysis.

(E) Kaplan-Meier curve of bone metastasis development of control and VCAM-1 overexpressing CN34 cells (n = 10). *p < 0.05 (log-rank test).

(F) Representative BLI (day 125) and X-rays (day 154) of mice from (E). Arrows point to osteolytic lesions.

(G) Ectopic overexpression of VCAM-1 in MDA-MB-435 as detected by western blot analysis.

(H) Kaplan-Meier curve of bone metastasis development of control and VCAM-1-overexpressing MDA-MB-435 cells (n = 10). *p < 0.05 (log-rank test).

(I) Representative BLI (day 42) of mice from (H).

Validation of the Prometastatic Role of VCAM-1 in Other Bone Metastasis Models

To further evaluate whether VCAM-1 is sufficient for bone metastasis, we overexpressed it in SCP6 and the revertant line PD2R. While ectopic expression of VCAM-1 was insufficient to confer bone-metastatic ability to SCP6 (Figures 2D and 2E), it was sufficient to promote the outgrowth of bone metastases formed by PD2R, which otherwise failed to further expand 50 days after injection (Figures 2F–2H). This result indicates the initial conversion from micrometastases to overt macrometastases required more than VCAM-1 upregulation in the genetic background of SCP6. Nevertheless, VCAM-1 overexpression alone is sufficient to rescue the metastatic property of PD2R, which is more closely related to PD1.

To test whether VCAM-1 function in promoting bone metastasis was restricted to MDA-MB-231, we used other bone metastasis models. Recently, the TM40D murine mammary tumor cell line was subjected to in vivo selection to establish the highly bone-metastatic TM40D-MB subline. Interestingly, *VCAM-1* was one of the 14 genes found to be significantly overexpressed in TM40D-MB (Li et al., 2008) (Figure 2I). We silenced *VCAM-1* expression in TM40D-BM and observed dramatic reduction of bone metastasis (Figures 2I–2K).

We further tested the prometastatic function of VCAM-1 in several human breast cancer cell lines with mild bone-metastatic abilities. MCF7 is an estrogen receptor (ER)-positive cell line that generates slowly growing bone metastases in less than 20% of inoculated mice (Lu et al., 2009). Ectopic expression of VCAM-1 in MCF7 led to formation of osteolytic bone metastases in 69% of mice (Figures 3A–3C). Two ER-negative cancer cell lines were tested in addition to the MDA-MB-231 derivatives (also an ER-negative model). CN34 was recently isolated from pleural effusion and showed marginal potential to form bone metastasis (Zhang et al., 2009). VCAM-1 overexpression

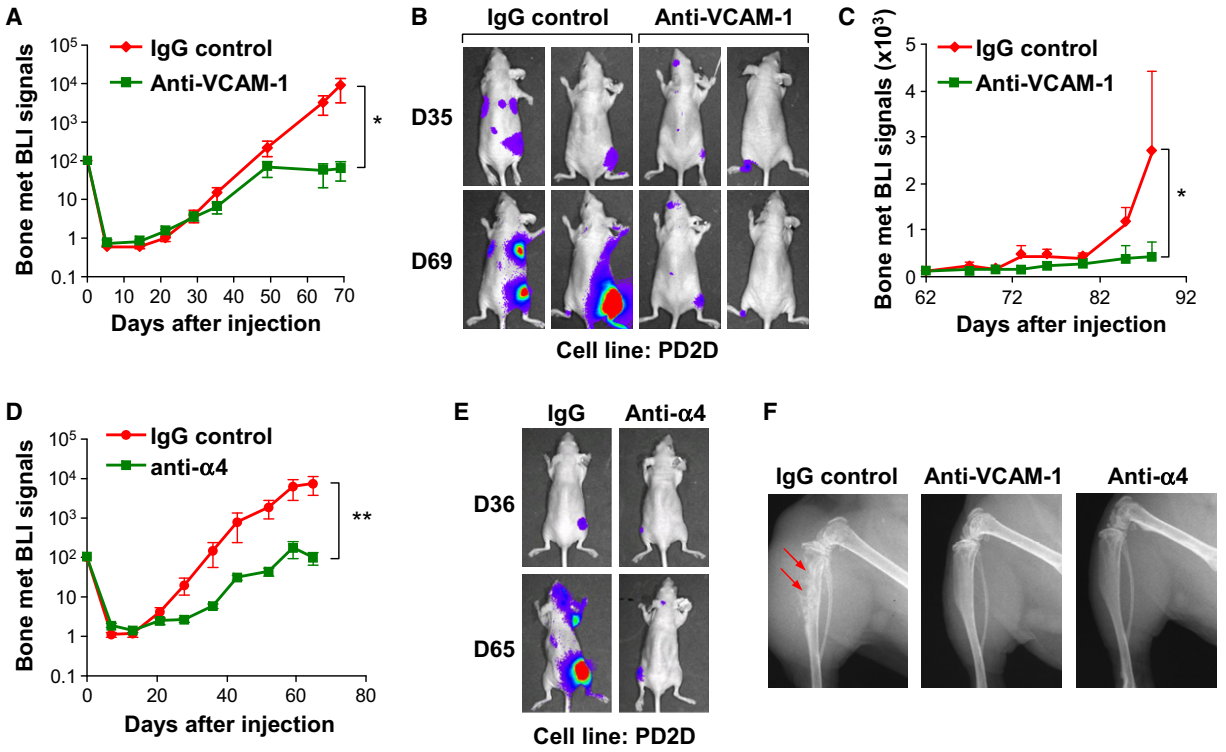

Figure 4. Antibody Therapy Targeting VCAM-1 and Integrin α4 Inhibits Bone Metastasis

(A) BLI curves of bone metastasis development by PD2D cells in nude mice with control IgG or anti-VCAM-1 (clone P3C4) treatment started from day 10. Data represent the mean ± SEM (n = 6). *p < 0.05 (Mann-Whitney test).

(B) Representative BLI of mice treated with IgG or anti-VCAM-1 antibodies.

(C) BLI curves of bone metastasis progression by PD2D cells with control IgG or anti-VCAM-1 treatment started from day 62. BLI signals were normalized to day 62 to facilitate comparison. Data represent the mean ± SEM (n = 6). *p < 0.05 (Mann-Whitney test).

(D) BLI curves of bone metastasis development by PD2D cells with control IgG or anti-α4 (clone PS/2) treatment started from day 0 until day 21. Data represent the mean ± SEM (n = 10). **p < 0.01 (Mann-Whitney test).

(E) Representative BLI of mice treated with IgG or anti-α4.

(F) X-ray of PD2D-injected mice treated with anti-VCAM-1 (A) or anti-α4 (D) at the end of experiments. Arrows point to osteolytic lesions. See also Figure S3.

substantially increased the osteolytic bone metastasis of CN34 cells (Figures 3D–3F). Finally, MDA-MB-435, coexpressing both epithelial and melanocytic markers (Chambers, 2009), contains discernable level of VCAM-1 (Figure 3G) and displays mild aggressiveness to bone (Lu et al., 2009). VCAM-1 overexpression further enhanced bone colonization efficiency of MDA-MB-435 (Figures 3H and 3I). It should be noted that the prometastasic effect of VCAM-1 overexpression in CN34 was less dramatic compared with MCF7 and MDA-MB-435, probably reflecting the requirement for other genes in CN34 to colonize the bone more efficiently. Taken together, we conclude that VCAM-1 has a general prometastatic function in bone metastasis.

Therapeutic Targeting of VCAM-1 or Cognate Receptor by Antibodies

To evaluate the therapeutic benefit of targeting VCAM-1 using a more clinically applicable approach, we used a previously developed monoclonal antibody (clone P3C4) capable of blocking VCAM-1 binding activity (Dittel et al., 1993). To test the antimetastatic activity of the antibody, mice were treated 10 days after the intracardiac injection of PD2D cells to mimic adjuvant therapy. Mice treated with control immunoglobulin G (IgG) developed aggressive bone metastases that grew continuously, whereas those treated with anti-VCAM-1 only developed a low level of bone metastasis burden that reached a plateau within 50 days (Figures 4A and 4B). Dramatically diminished metastasis was also achieved when antibody was applied following an early adjuvant protocol (Figures S3A–S3C). To evaluate whether VCAM-1 antibody can inhibit established metastases, mice were treated with antibody 62 days after cell injection, and again demonstrated efficacy in impeding metastasis growth (Figure 4C).

VCAM-1 is a ligand for integrin α4β1 and only binds weakly to integrin α4β7 (Springer, 1994). Because neither SCP6 nor PD cells express α4 (Figure S3D), in vivo VCAM-1-integrin interaction, if existent, is expected to occur between tumor and murine host cells. Because α4 is the common integrin subunit, we used a previously developed neutralizing monoclonal antibody against murine α4, clone PS/2 (Miyake et al., 1991). As expected, mice injected with PD2D and treated with anti-α4 showed less bone metastasis formation and better preserved bone structure (Figures 4D and 4E).

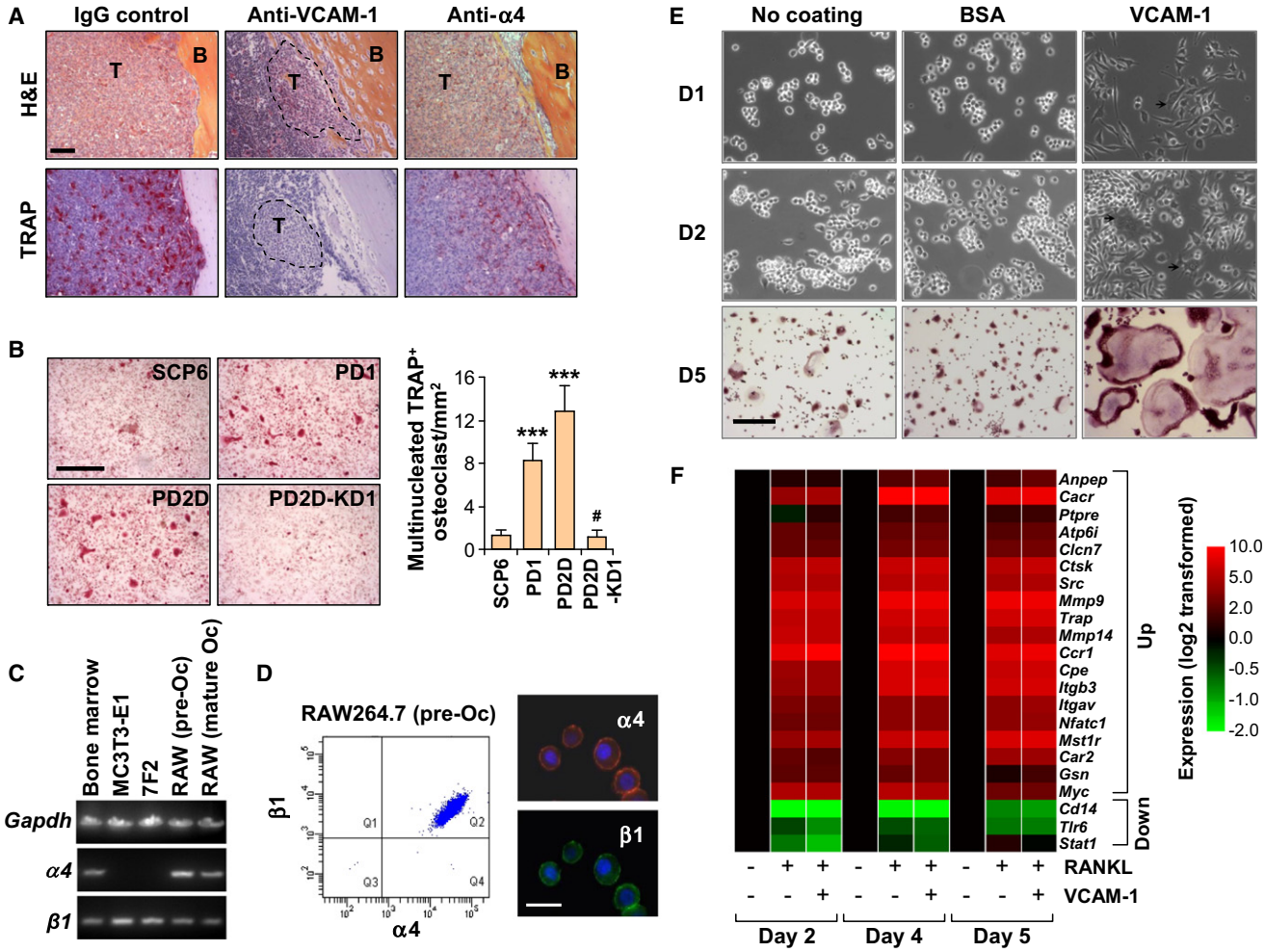

Figure 5. VCAM-1 Promotes Osteoclast Activation by Direct Interaction with Preosteoclasts

(A) Hematoxylin and eosin (H&E) and TRAP staining of hindlimb long bones showing tumor (T, demarcated by dotted line), bone (B), and TRAP$^+$ (red) osteoclasts. Mice were injected with PD2D, and samples were obtained from Figure 4F. Scale bar, 100 μm.

(B) In vitro osteoclastogenesis of murine bone marrow cocultured with different tumor cell monolayers. Mature osteoclasts were quantified as multinucleated TRAP$^+$ (red) cells. Data represent the mean ± SD. ***$p < 0.001$, $^{\#}p > 0.5$ (Student's t test and Mann-Whitney test). Scale bar, 250 μm.

(C) RT-PCR showing α4β1 expression in RAW264.7 before as well as after induced differentiation, but not in osteoblast cell lines (MC3T3-E1 and 7F2). Murine bone marrow was used as a positive control.

(D) Surface expression of α4β1 by RAW264.7 revealed by FACS staining. Scale bar, 25 μm.

(E) RANKL-induced RAW264.7 differentiation on precoated plates. Arrows indicate early formation of multinucleated cells. TRAP staining on day 5 showed morphologically larger osteoclasts in VCAM-1-coated plate. Scale bar, 100 μm.

(F) Expression pattern of known osteoclast differentiation markers in RAW264.7 cultured with or without VCAM-1-coating in the presence or absence of RANKL induction. The markers, quantified by quantitative RT-PCR, include known upregulated (Up) and downregulated (Down) genes during osteoclast differentiation. See also Figure S4.

VCAM-1 Promoting Osteoclast Activation in Bone Metastasis

Because highly bone-metastatic PD cells do not possess a significantly higher proliferation rate than the dormant SCP6 and weakly metastatic PD2R cells in vitro (Figure S4A), we investigated the potential mechanism for VCAM-1 in conferring the growth advantage of PD cells in the bone microenvironment. The vicious cycle in bone metastasis, mediated by the activation of bone-degrading osteoclasts, has been well known to play a central role in determining the osteolytic nature and aggressiveness of breast cancer bone metastasis (Weilbaecher et al., 2011). We hypothesized that VCAM-1 promotes bone metastasis through activating osteoclasts, thereby instigating the establishment of the vicious cycle. First, we examined osteoclast activity in IgG or antibody-treated bone metastases (adjuvant therapy protocol) by staining the osteoclast marker tartrate-resistant acid phosphatase (TRAP). TRAP$^+$ osteoclasts were abundantly enriched in the bone metastases formed by PD2D in the IgG-treated mice (Figure 5A). Other parts of the bone did not have elevated number of TRAP$^+$ osteoclasts, suggesting a local osteoclast-inducing milieu by PD2D cells (Figure S4B). Dramatically weaker osteoclast activity was observed

in metastases treated with anti-VCAM-1 or anti-α4 (Figure 5A; Figure S5B). Metastases formed by PD2R with ectopic VCAM-1 overexpression also contained numerous TRAP$^+$ osteoclasts (Figure S4C).

To directly test whether VCAM-1 expressed on tumor cells could influence osteoclast differentiation, we cocultured SCP6 or VCAM-1$^+$ PD cells with primary murine bone marrow cells under conditions inductive of osteoclast differentiation. Significantly, more TRAP$^+$ multinucleated osteoclasts formed when cocultured with PD1 or PD2D compared to SCP6 (Figure 5B). VCAM-1 KD diminished the ability of PD2D to enhance osteoclastogenesis (Figure 5B). Bone marrow contains a heterogeneous population of cells. VCAM-1 may interact directly with osteoclast progenitors to influence their differentiation, or may instead act through an intermediate cell type, such as osteoblasts (Weilbaecher et al., 2011). To distinguish these two possibilities, we analyzed the expression pattern of α4β1 in two murine osteoblast cell lines (MC3T3-E1 clone 4 and 7F2) and one murine preosteoclast cell line (RAW264.7) using RT-PCR (Figure 5C) and flow cytometry (Figure 5D). Although β1 was ubiquitously expressed, α4 was only expressed by RAW264.7 (before and after differentiation). Therefore, tumor cells and preosteoclasts, given physical proximity, could interact directly via VCAM-1-α4β1 binding. This result allowed us to simplify the analysis of VCAM-1 function in osteoclastogenesis by precoating culture plates with recombinant VCAM-1 before seeding RAW264.7. VCAM-1 coating led to earlier multinucleation and eventually larger cell size with more nuclei in mature TRAP$^+$ osteoclasts (Figure 5E).

One obvious explanation for the enhanced multinucleation would be that VCAM-1 induced differentiation. However, when we examined the expression of 19 upregulated and 3 downregulated genes known to be tightly and functionally correlated with osteoclast differentiation (Yang et al., 2008), VCAM-1 coating and BSA coating showed similar patterns during osteoclast differentiation (Figure 5F). In addition, VCAM-1 coating did not change the level of phosphorylated Src, extracellular-regulated kinase, or Akt in RAW264.7 (Figure S4D). Therefore, the enhanced osteoclast multinucleation may simply be the result of more attachment of preosteoclasts to a VCAM-1-coated surface and more cell fusion favored by closer cell juxtaposition. Translating this hypothesis in vivo, soluble VCAM-1 (sVCAM-1) and membrane-bound VCAM-1 on tumor cells may recruit and arrest more osteoclast progenitors to provide an osteoclastic niche.

VCAM-1-Mediated Attraction of Osteoclast Progenitors

sVCAM-1 produced by PD cells was readily detectable in conditioned medium as well as in serum from tumor-bearing mice (Figure S4E), suggesting a potential role of VCAM-1 in recruiting circulating osteoclast precursors to promote osteoclastogenesis. We tested this hypothesis by first showing that recombinant VCAM-1 is a chemoattractant for preosteoclasts by a standard checkerboard analysis (Figure S5A). VCAM-1-α4β1 binding was essential for chemoattraction (Figure 6A), and sVCAM-1 secreted by tumor cells was able to attract preosteoclasts (Figure 6B). Second, we demonstrated a significantly higher adhesion rate of RAW264.7 cells to VCAM-1$^+$ PD2D cells than SCP6 or PD2D-KD1 (Figures S5B and S5C). Scanning electron microscopy revealed tight attachment of RAW264.7 cells to PD2D and loose juxtaposition to SCP6 or PD2D-KD1 (Figure 6C). Next, we attempted to analyze in vivo metastases for evidence of osteoclast progenitor attraction. A prerequisite for host cells to interact with VCAM-1$^+$ tumor cells is α4β1 expression. Murine bone marrow analysis revealed α4$^+$β1$^+$ and α4$^-$β1$^+$ subpopulations in the CD11b$^+$ monocytes (Figure 6D). CD11b$^+$ monocytes are known to contain osteoclast progenitors (Ishii et al., 2009). Intriguingly, the α4$^+$β1$^+$ subpopulation differentiated into significantly more multinucleated TRAP$^+$ osteoclasts upon macrophage-colony stimulating factor (M-CSF) and receptor activator for NF-κB ligand (RANKL) treatment (Figure 6D). Therefore, VCAM-1$^+$ PD cells may attract the α4$^+$β1$^+$ osteoclast progenitors in vivo to promote bone metastasis. Indeed, we observed the enrichment of osteoclast progenitors, in particular the α4$^+$β1$^+$ subpopulation, in bone metastases formed by VCAM-1$^+$ PD cells (Figures 6E and 6F). Conversely, mice with PD2D bone metastases contained a lower percentage of CD11b$^+$ cells in the peripheral blood (Figure 6G).

If bone metastases attract and immobilize osteoclast progenitors through VCAM-1 activity, transient blocking of VCAM-1 by neutralizing antibodies should release the attached cells from the tumor. However, this hypothesis is difficult to test with the current methodologies because FACS analysis of bone marrow and blood composition may be complicated by VCAM-1-dependent physiological homing of hematopoietic cells (Papayannopoulou et al., 2001). Furthermore, it is difficult to provide information on dynamic cell movement using standard histology. To overcome these technical challenges, we developed the real-time imaging technique EviBoM by incorporating BLI with multicolor multiphoton laser-scanning microscopy. To simultaneously detect tumor cells and stromal cells, we stably expressed mKeima (Kogure et al., 2006) to label tumor cells and generated nude mice with enhanced green fluorescent protein (EGFP)-labeled monocytes by crossing CX_3CR1-EGFP knock-in mice (Jung et al., 2000) with nude mice. mKeima showed strong red fluorescence intensity and superior spectral overlap with EGFP at wavelengths from 900 to 1000 nm, allowing simultaneous detection of mKeima$^+$ tumor cells and EGFP$^+$ monocytes (Figure S5D). After the formation of osteolytic bone metastasis detected by whole mouse BLI, we dissected the long bone, identified the location of metastasis by ex vivo BLI, and embedded the BLI-positive bone section in agarose. We adapted a previously described method for imaging GFP$^+$ hematopoietic stem cells ex vivo in the mouse long bone (Xie et al., 2009) and analyzed the dynamics of tumor-monocyte interaction in bone metastasis (Figure 6H). Using EviBoM, we found that movement velocity of CX_3CR1-EGFP$^+$ monocytes in the area of PD2D bone metastases was significantly increased after anti-VCAM-1 antibody treatment (Figures 6I and 6J; Movies S1 and S2), suggesting the release of VCAM-1-mediated cell-cell adhesion.

VCAM-1 Overexpression Is Dependent on NF-κB Signaling

We tested several possible mechanisms for the activation of VCAM-1 expression. We first ruled out gene copy number change based on array CGH analysis at the *VCAM-1* locus (Figure S1B) and quantitative PCR (data not shown). Next, we

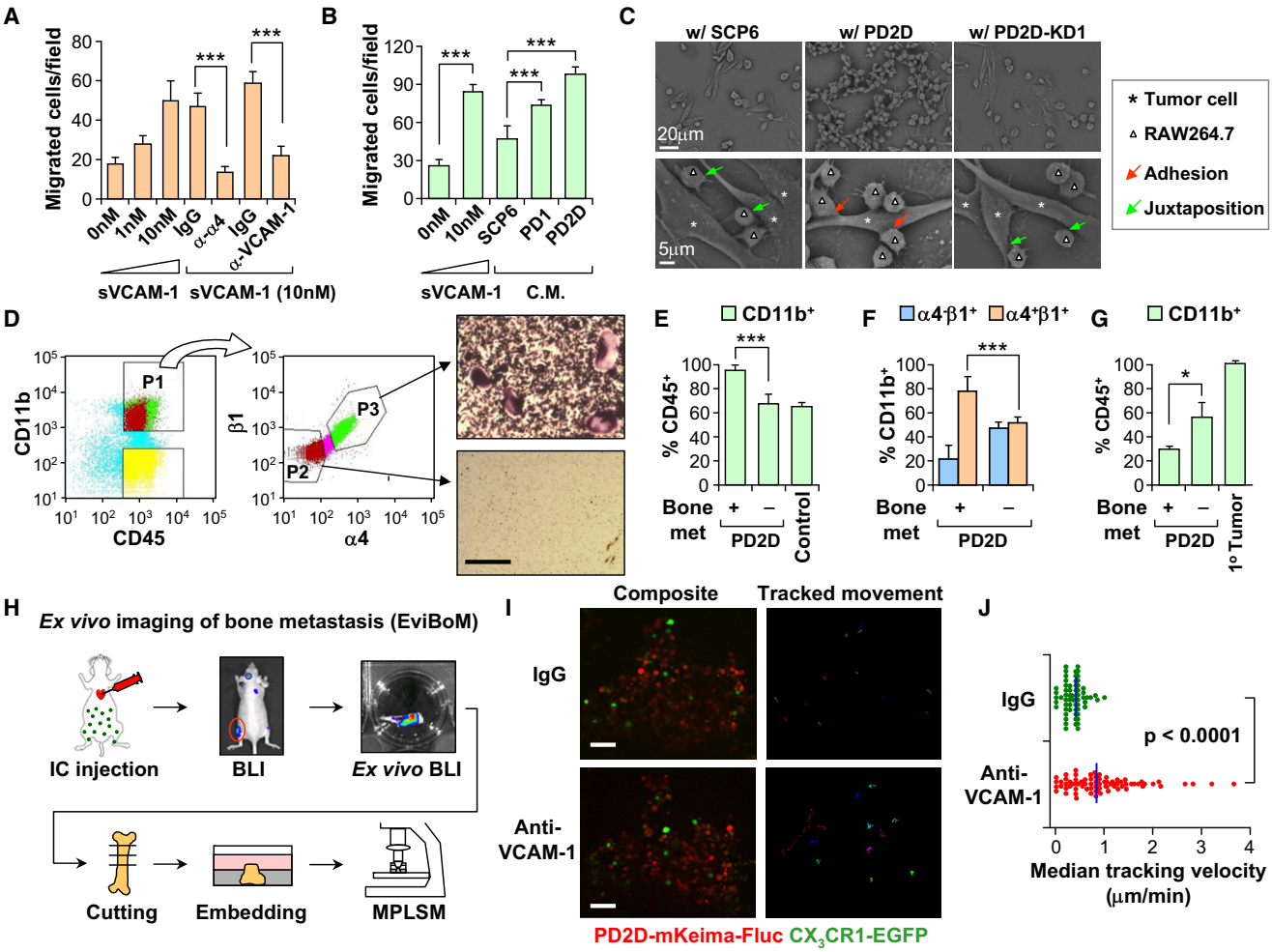

Figure 6. VCAM-1-Mediated Attraction of Osteoclast Progenitors

(A) Chemotaxis of RAW264.7 to sVCAM-1 blocked by anti-VCAM-1 or anti-α4 antibodies.

(B) Chemotaxis of RAW264.7 to tumor-conditioned medium. In (A) and (B), data represent the mean ± SD. ***$p < 0.001$ (Student's t test).

(C) Scanning EM showing adhesion of RAW264.7 to PD2D but not to SCP6 or VCAM-1-silenced PD2D.

(D) FACS of murine bone marrow showing $\alpha4^+\beta1^+$ (P3) and $\alpha4^-\beta1^+$ (P2) cells in $CD45^+CD11b^+$ monocytes (P1). Sorted P3, but not P2, differentiated into $TRAP^+$ osteoclasts under induction. Scale bar, 500 μm.

(E) FACS quantification of $CD11b^+$ monocytes in $CD45^+$ bone marrow leukocytes of mice injected with PD2D with or without bone metastases formed, as well as of age-matched mice without injection (control).

(F) FACS quantification of $\alpha4^+\beta1^+$ and $\alpha4^-\beta1^+$ subpopulations of $CD11b^+$ monocytes in bone marrow of mice injected with PD2D with or without bone metastases formed.

(G) FACS quantification of $CD11b^+$ monocyte population in $CD45^+$ peripheral blood leukocytes of mice injected with PD2D with or without bone metastases formed, as well as of age-matched mice with established PD2D primary tumors. In (E), (F), and (G), the percentage was reported after excluding tumor cells (positive for human HLA-ABC), if they exist. Data represent the mean ± SD. *$p < 0.05$, ***$p < 0.001$ (Student's t test).

(H) Experimental flow of EviBoM. Green dots represent monocytes expressing the CX_3CR1-EGFP knock-in gene.

(I) Representative EviBoM image frames and tracked movement of CX_3CR1-$EGFP^+$ monocytes with IgG or anti-VCAM-1 ex vivo treatment. Scale bar, 30 μm.

(J) Comparison of median tracking velocity of CX_3CR1-$EGFP^+$ monocytes in (I). Black bar represents the median of all data (Student's t test). See also Figure S5, Movies S1 and S2.

hypothesized that the signaling pathways essential for driving VCAM-1 upregulation are constitutively active in VCAM-1^+ PD cells. Previous studies on VCAM-1 regulation identified multiple regulatory pathways or factors, including NF-κB, p300/CBP, protein kinase C, mitogen-activated protein kinase kinase 1/2, phospholipase C, mammalian target of rapamycin, phosphatidylinositol 3-kinase, epidermal growth factor receptor, and miR-126 (Iademarco et al., 1992; Lee et al., 2008; Minami and Aird, 2001). To identify the pathway that might be involved in VCAM-1 upregulation, we used pharmacological inhibitors to inactivate each of these pathways in PD1 and PD2D and looked for consistent decrease of VCAM-1 expression (Figure S6A). Two pathways known to be important for bone metastasis, Src (Zhang et al., 2009) and transforming growth factor β (Kang et al., 2005), were also analyzed pharmacologically (Figure S6B). Among these inhibitors that we tested, only two

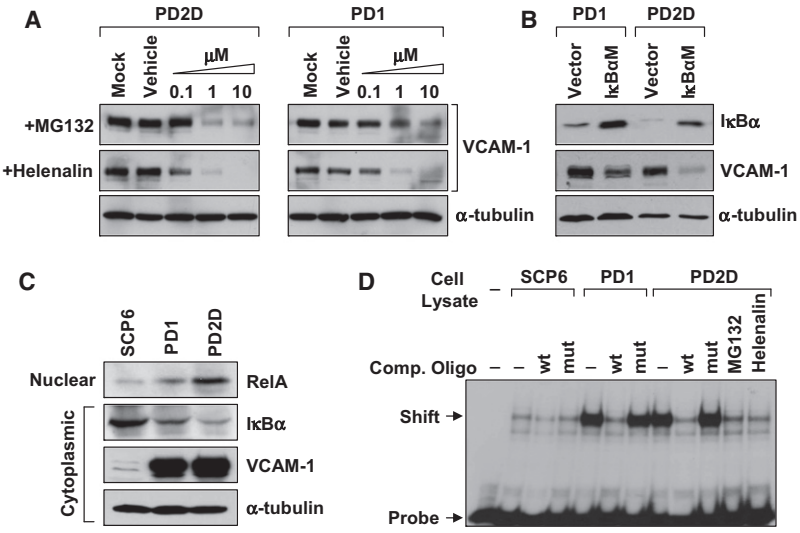

Figure 7. VCAM-1 Upregulation Is Dependent on NF-κB Activity

(A) Dose-dependent inhibition of VCAM-1 expression by NF-κB pathway inhibitors MG132 and helenalin as detected by western blot analysis.

(B) Inhibition of VCAM-1 expression by ectopic IκBαM expression as detected by western blot analysis.

(C) Differential abundance of nuclear RelA and cytoplasmic IκBα in SCP6 and VCAM-1$^+$ PD cells as detected by western blot analysis.

(D) EMSA showing stronger band shift in PD1 and PD2D compared with SCP6. Wild-type competitive probe (wt) and inhibitors MG132 and helenalin, but not mutated competitive probe (mut), blocked radioactive NF-κB-specific probe binding. See also Figure S6.

inhibitors of the NF-κB pathway, MG132 (Fiedler et al., 1998) and helenalin (Lyss et al., 1998), blocked VCAM-1 expression at 0.1-1 μM concentration (Figure 7A; Figure S6A). To further confirm the role of NF-κB signaling in sustaining VCAM-1 expression, we genetically blocked the canonical NF-κB signaling with enforced expression of IκBαM, a dominant-negative form of NF-κB inhibitor α (IκBα) (Brown et al., 1995). IκBαM effectively reduced the VCAM-1 level (Figure 7B). Consistently, PD cells contained less IκBα in the cytoplasm and more RelA in the nucleus compared with SCP6 (Figure 7C). Direct evidence of increased NF-κB activity in PD cells was shown by electrophoretic mobility shift assay (EMSA) (Figure 7D). To test whether ectopic stimulation of NF-κB activity can drive VCAM-1 expression in SCP6, we treated SCP6 with tumor necrosis factor α, which is a known activator of NF-κB signaling, and observed a significant increase of *VCAM-1* messenger RNA level, yet the level was still dramatically lower than that in PD cells (Figures S6C and S6D). This result suggests other mechanisms may function cooperatively with NF-κB or independently to activate *VCAM-1* expression.

VCAM-1 Expression Associated with Clinical Early Recurrence

To evaluate the clinical importance of VCAM-1 in breast cancer, especially in the context of recurrence, we analyzed a breast cancer microarray dataset containing metastasis relapse information (Wang et al., 2005). The proportional relapse rate plot showed the typical biphasic distribution of breast cancer relapses with 30 months as the peak (Figure 8A) (Stearns et al., 2007). When VCAM-1 levels were compared between early and late recurrence groups using 30 months as a cutoff to stratify patients, higher VCAM-1 expression was significantly associated with early relapse (Figure 8B). To corroborate conclusion from in silico analysis, we stained VCAM-1 in a breast cancer tissue microarray (TMA) that contains 170 samples (Hu et al., 2009). Higher VCAM-1 expression in cancerous tissue was again correlated with early relapse (Figure 8C). These findings validated the clinical significance of VCAM-1 overexpression in early relapse of breast cancer.

DISCUSSION

Significant progress has been made to elucidate the molecular mechanisms of the multistep metastasis cascade. However, the mechanism underlying metastatic dormancy and relapse from the dormancy remains one of most challenging but also clinically relevant questions (Aguirre-Ghiso, 2007; Goss and Chambers, 2010). Our characterization of a bone metastasis mouse model has shed light on the molecular understanding of dormancy by showing that VCAM-1 is an essential protein that reactivates indolent micrometastasis in the bone microenvironment (Figure 8D).

A Metastasis Dormancy Animal Model

The most frequent sites of breast cancer metastasis include bone, lung, liver, and brain. Metastasis relapse can occur in any of these organs, and several attempts have been made to model metastasis dormancy in these sites. Survival of tumor cells during bone metastasis latency was linked to Src activity (Zhang et al., 2009). Progression of lung micrometastasis to macrometastasis in the transgenic MMTV-PyMT model was shown to be triggered by angiogenesis (Gao et al., 2008). Solitary tumor cells in the liver were visualized after intravenous injection of a murine mammary carcinoma cell line (Naumov et al., 2002). However, these models did not investigate the spontaneous in vivo activation of indolent micrometastasis, which represents the last phase of transition from dormancy to overt metastasis.

Our serendipitous observation of rare macrometastatic outgrowths after a long-term latency in mice allowed us to isolate reactivated cancer cells and compare them with the indolent parental cells to identify gene expression variations that may have led to the escape from dormancy. The transition from indolent growth to overt metastasis, as observed in our model, occurs in patients with metastasis recurrence many years after mastectomy. However, it is currently not feasible to prospectively isolate a tumor cell predicted to escape dormancy from a heterogeneous pool of disseminated tumor cells in patients. In fact, even in basic research, studies on in vivo metastasis dormancy are complicated by the heterogeneous growth properties of most cancer cell lines (Townson and Chambers, 2006): the behavior and characteristics of the minor dormant subpopulations are masked by the coexisting actively

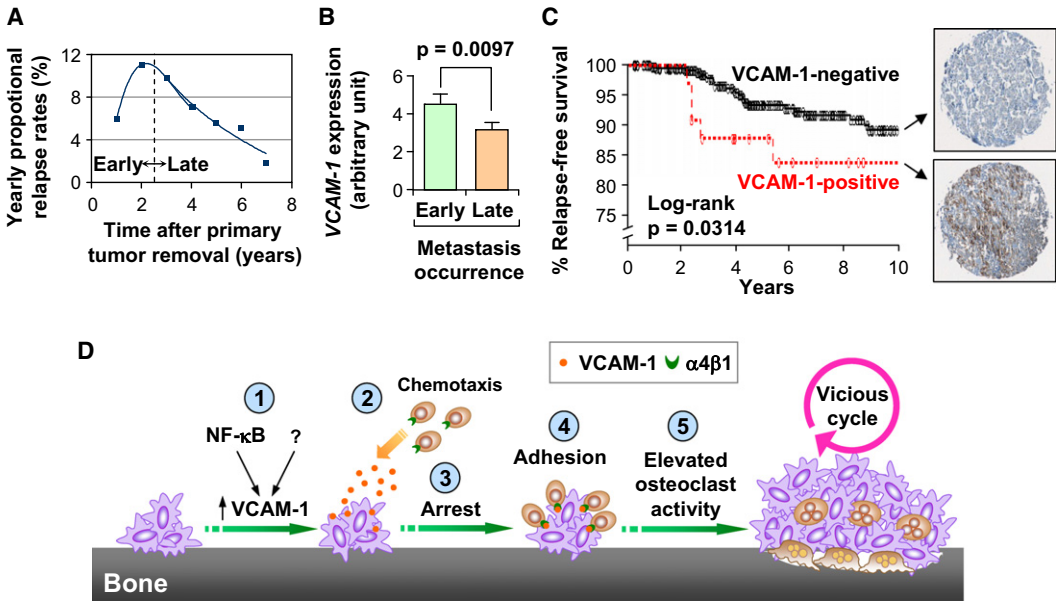

Figure 8. VCAM-1 Expression Is Associated with Clinical Early Recurrence

(A) Bimodal pattern of metastasis relapse in a breast cancer cohort (Wang et al., 2005). Dotted line separates early and late relapse at 30 months, the peak of the curve.

(B) VCAM-1 is expressed at a higher level in the early compared with the late metastasis relapse group. Data represent the mean ± SEM (Student's t test).

(C) VCAM-1 expression correlates with early recurrence in a breast cancer TMA. Also shown are representative breast carcinoma TMA samples stained for VCAM-1.

(D) A schematic model for the function of VCAM-1 in the transition from dormant micrometastasis to macrometastasis in bone. Incidental activation of VCAM-1, a process possibly dependent on NF-κB signaling and other unidentified mechanisms (1), in micrometastasis arrests α4β1-positive osteoclast progenitors through paracrine chemotaxis (2) and adhesion (3). This leads to a localized increase of the osteoclast progenitor population and increased mature osteoclast activity (4). Activated osteoclasts resorb the bone and instigate the vicious cycle of bone metastasis (5).

proliferating cells. These difficulties highlight the merit of our model. Because of the relatively homogeneous nature of the parental cell SCP6 (derived from a single clone) and the close relatedness of SCP6 with PD sublines, the genome-wide comparison of dormant and reactivated cells is particularly informative. Indeed, we identified VCAM-1 from this model as a key player in metastatic progression from dormancy.

A Functional Role for VCAM-1 in Activating Indolent Micrometastasis

Our mechanistic investigation of the function of VCAM-1 in promoting the escape from dormancy revealed its connection with osteoclastogenesis. By creating a "molecular sink" to attract circulating monocytic precursors of osteoclasts through VCAM-1-α4β1 interactions, VCAM-1 instigates a vicious cycle of bone destruction and tumor expansion. As such, VCAM-1 serves as an example of how shifting the physiological process of bone homeostasis can facilitate the expansion of nascent bone metastasis. However, we should mention that, in contrast to other previously identified bone metastasis factors such as Jagged1 (Sethi et al., 2011), VCAM-1 is not sufficient for osteoclast differentiation, as neither RAW264.7 cells nor murine bone marrow cocultured with VCAM-1$^+$ PD cells or plated on a VCAM-1-coated surface underwent differentiation without RANKL (data not shown). In addition, although it appears that, in this particular model system, VCAM-1 is likely to be a key factor for the recruitment of preosteoclasts to nascent bone micrometastasis, we do not rule out other chemoattractants playing contributing roles to this process. It is possible that such factors were upregulated in PD cells posttranscriptionally or posttranslationally, which could not be captured by our microarray analysis. We also want to point out a possible and unexplored regulatory checkpoint of VCAM-1 availability in our system, which is the proteolysis and shedding of sVCAM-1 from tumor cell membranes through the activity of metalloproteinases (Garton et al., 2003).

It is well established that α4β1 is important in bone marrow homing and retention of hematopoietic stem cells through its binding to VCAM-1 expressed in bone marrow endothelial and stromal cells (Papayannopoulou et al., 2001). It is reasonable to speculate that the interaction between VCAM-1 and α4β1 is also part of the program regulating monocyte retention in bone marrow. In support of this hypothesis, *VCAM-1*-deficient mice showed elevated blood mononuclear leukocytes, possibly due in part to the reduced retention of these cells in the bone marrow (Gurtner et al., 1995). Therefore, it is conceivable that breast cancer cells, by upregulating VCAM-1, could imitate the marrow endothelial and stromal cells to locally retain high density of monocytes as the source of osteoclast differentiation.

We noted that even with the inhibition of VCAM-1, PD2D cells could still expand more than 10-fold to form a micrometastasis with probably a few hundreds cells (Figures 4A and 5A). Our evidence suggests that VCAM-1 is crucial for the expansion of indolent bone micrometastasis but is dispensable for the survival

and initial growth of solitary tumor cells, the immediate step of metastatic colonization after seeding. On the other hand, a recent report showed that binding of VCAM-1-overexpressing tumor cells to macrophages directly promotes signal flow through the PI3K-Akt pathway for the survival of breast cancer cells that infiltrate the lung, but is not required for the immediate survival of those that seed the bone marrow (Chen et al., 2011). Nevertheless, in tissue samples of overt metastasis lesions from breast cancer patients, VCAM-1 was found to be overexpressed in both lung and bone metastases (Chen et al., 2011). Taken together, these findings indicate that VCAM-1 plays important functions in promoting metastatic colonization in both bone and lung, although at different stages and through different mechanisms. Therefore, blocking VCAM-1 activity may represent an effective strategy to prevent the formation of overt metastasis in both bone and lung, two of the most frequent sites of distant relapse in breast cancer.

Inflammation, NF-κB Signaling, and VCAM-1 Regulation

Inflammation has long been hypothesized to be linked to cancer based on the pathological infiltration of leukocytes in neoplastic tissue as well as the association of chronic inflammation and infectious agents with cancer (Grivennikov et al., 2010). An inflammatory microenvironment, triggered by an infection, trauma, or stress, has been proposed to waken dormant tumor cells (Fehm et al., 2008), although experimental evidence is lacking. The canonical NF-κB pathway plays a central role in mediating the effect of inflammation on tumor progression (Grivennikov et al., 2010). Here, we found that VCAM-1 expression in PD cells is dependent on constitutive NF-κB activity. Therefore, our study suggests a possible link between the NF-κB pathway and recurrent bone metastasis, although direct evidence showing the causal role of N-FκB activation in the metastatic progression from dormancy is lacking and warrants further experimental validation. Supporting the functional significance of the NF-κB pathway in bone metastasis, NF-κB has been shown to stimulate granulocyte M-CSF expression in tumor cells to promote osteoclastogenesis and bone metastasis (Park et al., 2007). Other factors regulated by NF-κB may also contribute to metastasis progression, such as CXCL1 and CSF-1 which are also expressed by PD cells, although not at a significantly higher level when compared with SCP6 (data not shown). The other two well-known NF-κB targets, CCL2 and CCL5, are expressed at negligible levels in PD cells.

Single-Cell Imaging of Tumor-Stromal Interactions in Bone Metastasis

A significant technical contribution of our study is the development of EviBoM (Figure 6H) imaging technique for bone metastasis research. Optical intravital imaging has attracted increasing interest in the field of metastasis research, because it offers high spatial and temporal resolution in vivo and enables direct observation of metastasis at the single cell resolution (Sahai, 2007). Intravital imaging has lent strength to tumor dormancy research in studies characterizing tumor cell fates at secondary organs (Kienast et al., 2010; Naumov et al., 2002). Mouse skull was previously used as the site to study leukemia bone metastasis with in vivo confocal imaging (Sipkins et al., 2005). However, metastases in long bones (in particular, femur and tibia of the legs) are much more commonly associated with clinical and experimental bone metastasis. We developed EviBoM to provide real-time observation of cell movement in long bone metastases, although it is still in an ex vivo setting. A limitation of the current method is that osteoclast progenitors only represent a fraction of the GFP^+ cells in the CX_3CR1-EGFP mice. More lineage-specific labeling will improve the application of EviBoM and facilitate mechanistic investigation and preclinical drug development for bone metastasis.

EXPERIMENTAL PROCEDURES

Tumor Xenografts and Analysis

All procedures involving mice were approved by the Institutional Animal Care and Use Committee of Princeton University. Intracardiac injections to generate bone metastases was performed in 4-week-old, female nude mice (National Cancer Institute) as described (Lu and Kang, 2009), with the exception of TM40D-BM, which was injected into BALB/c mice (National Cancer Institute). Development of metastasis in bone was monitored by BLI with the IVIS 200 Imaging System (Caliper Life Sciences) and analyzed with the Living Image software as described (Lu and Kang, 2009). X-ray examination was performed as described (Kang et al., 2003).

Clinical Specimens

A breast cancer TMA composed of 170 primary tumors (Hu et al., 2009) was used in our association study. Breast tumor specimens used in the TMA were obtained from the Cancer Institute of New Jersey with informed consent from all subjects in accordance with the institutional review boards of Princeton University and the University of Medicine and Dentistry of New Jersey, and the samples were subsequently deidentified prior to analysis. More detailed information about immunohistochemical analysis of VCAM1-1 expression in TMA can be found in the Supplemental Information.

EviBoM

We stably labeled PD2D with retroviral vectors expressing firefly luciferase (cloned into pMSCVhygro) and mKeima (cloned into pMSCVpuro), and intracardiacally injected tumor cells into CX_3CR1-EGFP knock-in mice (The Jackson Laboratory) that had been crossed to harbor homozygous *nu* alleles. After detection of significant bone metastasis formation by BLI, we located the position of bone metastasis via ex vivo BLI, sectioned the bone with QwikStrip Serrated strip (Axis Dental), and embedded them into a thin layer of 1.5% low melting temperature agarose gel that is submerged in phenol red-free Dulbecco's modified Eagle's medium (Thermo Scientific) containing 1× penicillin-streptomycin and 10 mM HEPES (balancing pH). The bone sections were imaged under a customized upright multiphoton microscope built around a BX51 microscope (Olympus). More detailed methods can be found in the Supplemental Information.

Statistical Analysis

Results were reported as mean ± SD or mean ± SEM, indicated in the figure legend. Comparisons between Kaplan-Meier curves were performed using the log-rank test. Other comparisons were performed using unpaired two-sided Student's t test without equal variance assumption or nonparametric Mann-Whitney test.

ACCESSION NUMBERS

The raw and normalized microarray data have been deposited in the Gene Expression Ominbus database under accession number GSE20611.

SUPPLEMENTAL INFORMATION

Supplemental information includes six figures, one table, two movies, and Supplemental Experimental Procedures and can be found with this article online at doi:10.1016/j.ccr.2011.11.002.

ACKNOWLEDGMENTS

We thank S. Thiberge for two-photon microscopy analysis; C. DeCoste and M. Bisher for assistance with flow cytometry and electron microscopy; D. Medina and M. Zhang for TM40D cell lines; L. Cong, J. Friedman, and L. Goodell at Tissue Analytic Service Core of Cancer Institute of New Jersey for assistance with TMA analysis; and L. Mercatali, T. Ibrahim, D. Amadori, and M. Reiss for tissue analysis and helpful discussions. The Imaging Core Facility at the Lewis-Sigler Institute is supported by the Center Grant P50GM071508. Y.K. is a Champalimaud Investigator and a Department of Defense Era of Hope Scholar Award recipient. This research was additionally supported by grants from the Breast Cancer Alliance, Susan G. Komen for the Cure, the American Cancer Society, and the Brewster Foundation (to Y.K.) and from the Breast Cancer Research Foundation (to B.G.H.). J.M. is an Investigator of the Howard Hughes Medical Institute and is funded by grants from the National Institutes of health, the Kleberg Foundation, the Hearst Foundation, and the BBVA Foundation. X.L. is a recipient of the Harold W. Dodds Fellowship from Princeton University. Y.H. and B. T. are recipients of the DOD predoctoral fellowships.

Received: July 20, 2011
Revised: October 14, 2011
Accepted: November 2, 2011
Published online: December 1, 2011

REFERENCES

Aguirre-Ghiso, J.A. (2007). Models, mechanisms and clinical evidence for cancer dormancy. Nat. Rev. Cancer *7*, 834–846.

Braun, S., Vogl, F.D., Naume, B., Janni, W., Osborne, M.P., Coombes, R.C., Schlimok, G., Diel, I.J., Gerber, B., Gebauer, G., et al. (2005). A pooled analysis of bone marrow micrometastasis in breast cancer. N. Engl. J. Med. *353*, 793–802.

Brown, K., Gerstberger, S., Carlson, L., Franzoso, G., and Siebenlist, U. (1995). Control of I kappa B-alpha proteolysis by site-specific, signal-induced phosphorylation. Science *267*, 1485–1488.

Carter, R.A., and Wicks, I.P. (2001). Vascular cell adhesion molecule 1 (CD106): a multifaceted regulator of joint inflammation. Arthritis Rheum. *44*, 985–994.

Chambers, A.F. (2009). MDA-MB-435 and M14 cell lines: identical but not M14 melanoma? Cancer Res. *69*, 5292–5293.

Chambers, A.F., Groom, A.C., and MacDonald, I.C. (2002). Dissemination and growth of cancer cells in metastatic sites. Nat. Rev. Cancer *2*, 563–572.

Chen, Q., Zhang, X.H.-F., and Massagué, J. (2011). Macrophage binding to receptor VCAM-1 transmits survival signals in breast cancer cells that invade the lungs. Cancer Cell *20*, 538–549.

Cybulsky, M.I., Iiyama, K., Li, H., Zhu, S., Chen, M., Iiyama, M., Davis, V., Gutierrez-Ramos, J.-C., Connelly, P.W., and Milstone, D.S. (2001). A major role for VCAM-1, but not ICAM-1, in early atherosclerosis. J. Clin. Invest. *107*, 1255–1262.

Demicheli, R. (2001). Tumour dormancy: findings and hypotheses from clinical research on breast cancer. Semin. Cancer Biol. *11*, 297–306.

Demicheli, R., Abbattista, A., Miceli, R., Valagussa, P., and Bonadonna, G. (1996). Time distribution of the recurrence risk for breast cancer patients undergoing mastectomy: further support about the concept of tumor dormancy. Breast Cancer Res. Treat. *41*, 177–185.

Ding, Y.B., Chen, G.Y., Xia, J.G., Zang, X.W., Yang, H.Y., and Yang, L. (2003). Association of VCAM-1 overexpression with oncogenesis, tumor angiogenesis and metastasis of gastric carcinoma. World J. Gastroenterol. *9*, 1409–1414.

Dittel, B.N., McCarthy, J.B., Wayner, E.A., and LeBien, T.W. (1993). Regulation of human B-cell precursor adhesion to bone marrow stromal cells by cytokines that exert opposing effects on the expression of vascular cell adhesion molecule-1 (VCAM-1). Blood *81*, 2272–2282.

Fehm, T., Mueller, V., Marches, R., Klein, G., Gueckel, B., Neubauer, H., Solomayer, E., and Becker, S. (2008). Tumor cell dormancy: implications for the biology and treatment of breast cancer. APMIS *116*, 742–753.

Fiedler, M.A., Wernke-Dollries, K., and Stark, J.M. (1998). Inhibition of TNF-alpha-induced NF-kappaB activation and IL-8 release in A549 cells with the proteasome inhibitor MG-132. Am. J. Respir. Cell Mol. Biol. *19*, 259–268.

Gao, D., Nolan, D.J., Mellick, A.S., Bambino, K., McDonnell, K., and Mittal, V. (2008). Endothelial progenitor cells control the angiogenic switch in mouse lung metastasis. Science *319*, 195–198.

Garton, K.J., Gough, P.J., Philalay, J., Wille, P.T., Blobel, C.P., Whitehead, R.H., Dempsey, P.J., and Raines, E.W. (2003). Stimulated shedding of vascular cell adhesion molecule 1 (VCAM-1) is mediated by tumor necrosis factor-alpha-converting enzyme (ADAM 17). J. Biol. Chem. *278*, 37459–37464.

Goss, P.E., and Chambers, A.F. (2010). Does tumour dormancy offer a therapeutic target? Nat. Rev. Cancer *10*, 871–877.

Grivennikov, S.I., Greten, F.R., and Karin, M. (2010). Immunity, inflammation, and cancer. Cell *140*, 883–899.

Gurtner, G.C., Davis, V., Li, H., McCoy, M.J., Sharpe, A., and Cybulsky, M.I. (1995). Targeted disruption of the murine VCAM1 gene: essential role of VCAM-1 in chorioallantoic fusion and placentation. Genes Dev. *9*, 1–14.

Hu, G., Chong, R.A., Yang, Q., Wei, Y., Blanco, M.A., Li, F., Reiss, M., Au, J.L.S., Haffty, B.G., and Kang, Y. (2009). MTDH activation by 8q22 genomic gain promotes chemoresistance and metastasis of poor-prognosis breast cancer. Cancer Cell *15*, 9–20.

Iademarco, M.F., McQuillan, J.J., Rosen, G.D., and Dean, D.C. (1992). Characterization of the promoter for vascular cell adhesion molecule-1 (VCAM-1). J. Biol. Chem. *267*, 16323–16329.

Ishii, M., Egen, J.G., Klauschen, F., Meier-Schellersheim, M., Saeki, Y., Vacher, J., Proia, R.L., and Germain, R.N. (2009). Sphingosine-1-phosphate mobilizes osteoclast precursors and regulates bone homeostasis. Nature *458*, 524–528.

Jin, L., Yuan, R.Q., Fuchs, A., Yao, Y., Joseph, A., Schwall, R., Schnitt, S.J., Guida, A., Hastings, H.M., Andres, J., et al. (1997). Expression of interleukin-1beta in human breast carcinoma. Cancer *80*, 421–434.

Jung, S., Aliberti, J., Graemmel, P., Sunshine, M.J., Kreutzberg, G.W., Sher, A., and Littman, D.R. (2000). Analysis of fractalkine receptor CX(3)CR1 function by targeted deletion and green fluorescent protein reporter gene insertion. Mol. Cell. Biol. *20*, 4106–4114.

Kang, Y., Siegel, P.M., Shu, W., Drobnjak, M., Kakonen, S.M., Cordón-Cardo, C., Guise, T.A., and Massagué, J. (2003). A multigenic program mediating breast cancer metastasis to bone. Cancer Cell *3*, 537–549.

Kang, Y., He, W., Tulley, S., Gupta, G.P., Serganova, I., Chen, C.R., Manova-Todorova, K., Blasberg, R., Gerald, W.L., and Massagué, J. (2005). Breast cancer bone metastasis mediated by the Smad tumor suppressor pathway. Proc. Natl. Acad. Sci. USA *102*, 13909–13914.

Kienast, Y., von Baumgarten, L., Fuhrmann, M., Klinkert, W.E.F., Goldbrunner, R., Herms, J., and Winkler, F. (2010). Real-time imaging reveals the single steps of brain metastasis formation. Nat. Med. *16*, 116–122.

Klein, C.A. (2009). Parallel progression of primary tumours and metastases. Nat. Rev. Cancer *9*, 302–312.

Kogure, T., Karasawa, S., Araki, T., Saito, K., Kinjo, M., and Miyawaki, A. (2006). A fluorescent variant of a protein from the stony coral Montipora facilitates dual-color single-laser fluorescence cross-correlation spectroscopy. Nat. Biotechnol. *24*, 577–581.

Lee, C.W., Lin, C.C., Luo, S.F., Lee, H.C., Lee, I.T., Aird, W.C., Hwang, T.L., and Yang, C.M. (2008). Tumor necrosis factor-alpha enhances neutrophil adhesiveness: induction of vascular cell adhesion molecule-1 via activation of Akt and CaM kinase II and modifications of histone acetyltransferase and histone deacetylase 4 in human tracheal smooth muscle cells. Mol. Pharmacol. *73*, 1454–1464.

Li, Z., Schem, C., Shi, Y.H., Medina, D., and Zhang, M. (2008). Increased COX2 expression enhances tumor-induced osteoclastic lesions in breast cancer bone metastasis. Clin. Exp. Metastasis *25*, 389–400.

Lin, K.-Y., Lu, D., Hung, C.-F., Peng, S., Huang, L., Jie, C., Murillo, F., Rowley, J., Tsai, Y.-C., He, L., et al. (2007). Ectopic expression of vascular cell adhesion molecule-1 as a new mechanism for tumor immune evasion. Cancer Res. *67*, 1832–1841.

Lu, X., and Kang, Y. (2009). Efficient acquisition of dual metastasis organotropism to bone and lung through stable spontaneous fusion between MDA-MB-231 variants. Proc. Natl. Acad. Sci. USA *106*, 9385–9390.

Lu, X., Wang, Q., Hu, G., Van Poznak, C., Fleisher, M., Reiss, M., Massagué, J., and Kang, Y. (2009). ADAMTS1 and MMP1 proteolytically engage EGF-like ligands in an osteolytic signaling cascade for bone metastasis. Genes Dev. *23*, 1882–1894.

Lurquin, C., De Smet, C., Brasseur, F., Muscatelli, F., Martelange, V., De Plaen, E., Brasseur, R., Monaco, A.P., and Boon, T. (1997). Two members of the human MAGEB gene family located in Xp21.3 are expressed in tumors of various histological origins. Genomics *46*, 397–408.

Lyss, G., Knorre, A., Schmidt, T.J., Pahl, H.L., and Merfort, I. (1998). The anti-inflammatory sesquiterpene lactone helenalin inhibits the transcription factor NF-kappaB by directly targeting p65. J. Biol. Chem. *273*, 33508–33516.

Minami, T., and Aird, W.C. (2001). Thrombin stimulation of the vascular cell adhesion molecule-1 promoter in endothelial cells is mediated by tandem nuclear factor-kappa B and GATA motifs. J. Biol. Chem. *276*, 47632–47641.

Minn, A.J., Gupta, G.P., Siegel, P.M., Bos, P.D., Shu, W., Giri, D.D., Viale, A., Olshen, A.B., Gerald, W.L., and Massagué, J. (2005). Genes that mediate breast cancer metastasis to lung. Nature *436*, 518–524.

Miyake, K., Weissman, I.L., Greenberger, J.S., and Kincade, P.W. (1991). Evidence for a role of the integrin VLA-4 in lympho-hemopoiesis. J. Exp. Med. *173*, 599–607.

Naumov, G.N., MacDonald, I.C., Weinmeister, P.M., Kerkvliet, N., Nadkarni, K.V., Wilson, S.M., Morris, V.L., Groom, A.C., and Chambers, A.F. (2002). Persistence of solitary mammary carcinoma cells in a secondary site: a possible contributor to dormancy. Cancer Res. *62*, 2162–2168.

Osborn, L., Hession, C., Tizard, R., Vassallo, C., Luhowskyj, S., Chi-Rosso, G., and Lobb, R. (1989). Direct expression cloning of vascular cell adhesion molecule 1, a cytokine-induced endothelial protein that binds to lymphocytes. Cell *59*, 1203–1211.

Papayannopoulou, T., Priestley, G.V., Nakamoto, B., Zafiropoulos, V., and Scott, L.M. (2001). Molecular pathways in bone marrow homing: dominant role of alpha(4)beta(1) over beta(2)-integrins and selectins. Blood *98*, 2403–2411.

Park, B.K., Zhang, H., Zeng, Q., Dai, J., Keller, E.T., Giordano, T., Gu, K., Shah, V., Pei, L., Zarbo, R.J., et al. (2007). NF-kappaB in breast cancer cells promotes osteolytic bone metastasis by inducing osteoclastogenesis via GM-CSF. Nat. Med. *13*, 62–69.

Sahai, E. (2007). Illuminating the metastatic process. Nat. Rev. Cancer *7*, 737–749.

Sethi, N., Dai, X., Winter, C.G., and Kang, Y. (2011). Tumor-derived JAGGED1 promotes osteolytic bone metastasis of breast cancer by engaging notch signaling in bone cells. Cancer Cell *19*, 192–205.

Sipkins, D.A., Wei, X., Wu, J.W., Runnels, J.M., Côté, D., Means, T.K., Luster, A.D., Scadden, D.T., and Lin, C.P. (2005). In vivo imaging of specialized bone marrow endothelial microdomains for tumour engraftment. Nature *435*, 969–973.

Springer, T.A. (1994). Traffic signals for lymphocyte recirculation and leukocyte emigration: the multistep paradigm. Cell *76*, 301–314.

Stearns, A.T., Hole, D., George, W.D., and Kingsmore, D.B. (2007). Comparison of breast cancer mortality rates with those of ovarian and colorectal carcinoma. Br. J. Surg. *94*, 957–965.

Townson, J.L., and Chambers, A.F. (2006). Dormancy of solitary metastatic cells. Cell Cycle *5*, 1744–1750.

Wang, Y., Klijn, J.G.M., Zhang, Y., Sieuwerts, A.M., Look, M.P., Yang, F., Talantov, D., Timmermans, M., Meijer-van Gelder, M.E., Yu, J., et al. (2005). Gene-expression profiles to predict distant metastasis of lymph-node-negative primary breast cancer. Lancet *365*, 671–679.

Weilbaecher, K.N., Guise, T.A., and McCauley, L.K. (2011). Cancer to bone: a fatal attraction. Nat. Rev. Cancer *11*, 411–425.

Weinberg, R.A. (2008). The many faces of tumor dormancy. APMIS *116*, 548–551.

Wojtukiewicz, M.Z., Sierko, E., Zimnoch, L., Kozlowski, L., and Kisiel, W. (2003). Immunohistochemical localization of tissue factor pathway inhibitor-2 in human tumor tissue. Thromb. Haemost. *90*, 140–146.

Xie, Y., Yin, T., Wiegraebe, W., He, X.C., Miller, D., Stark, D., Perko, K., Alexander, R., Schwartz, J., Grindley, J.C., et al. (2009). Detection of functional haematopoietic stem cell niche using real-time imaging. Nature *457*, 97–101.

Yang, G., Zaidi, M., Zhang, W., Zhu, L.-L., Li, J., Iqbal, J., Varbanov, A., Gross, G., Phipps, R., Troen, B.R., and Sun, L. (2008). Functional grouping of osteoclast genes revealed through microarray analysis. Biochem. Biophys. Res. Commun. *366*, 352–359.

Zhang, X.H.F., Wang, Q., Gerald, W., Hudis, C.A., Norton, L., Smid, M., Foekens, J.A., and Massagué, J. (2009). Latent bone metastasis in breast cancer tied to Src-dependent survival signals. Cancer Cell *16*, 67–78.